Molecular Dynamics Determination of Thermodynamic Properties of Gold Clusters

Robin Loh, Matrikelnummer: 5203103

***Abstract*—This report details certain aspects of a Molecular Dynamics (MD) simulation which was used to determine thermodynamic properties of simulated gold clusters. The aspects of the simulation here presented give an overview of the entire simulation from the underlying physical models, to numerical integration, to techniques used to accelerate the computational process. Tests of the accuracy and validity of certain aspects of the simulation are presented as well. Finally, results of an experiment conducted to determine the thermodynamic properties of gold clusters of various sizes are presented and discussed.**

I Introduction

Understanding the dynamic behavior of molecules at the atomic level is not only a cornerstone of modern computational chemistry but also a key to unraveling the fundamental mechanisms that govern a wide range of physical, chemical, and biological processes. Molecular Dynamics (MD) simulations have emerged as an invaluable tool for providing insights into the behavior of molecular systems.

In this project, a basic MD simulation was implemented in C++ and used to investigate the heat capacity, melting point, and latent heat of simulated gold clusters of various sizes. The MD code uses the Velocity-Verlet integration scheme, and supports a basic Lennard-Jones (LJ) potential as well as an Embedded Atom Method (EAM) potential for gold clusters. It implements the Berendsen thermostat which may be used to equilibrate systems to desired temperatures. To speed computation, a neighbor-list search was implemented and the EAM potential is parallelized with this using a method of domain decomposition. This simulation was used to perform experiments to determine thermodynamic properties of gold clusters of varying sizes such as latent heat, melting point, and heat capacity.

The rest of the report is organized as follows: Sec. II details fundamental aspects of the simulation including the integration scheme and the two potentials outlined above. There we also determine suitable time-steps for each potential and discuss units. Sec. III then describes methods used to speed up computations, including a neighbor list search and parallelization. Results of the improvement on computation time and of the validity of the techniques are included as well. Sec. IV details the experimental methods used, which begins with a discussion of the Berendsen thermostat and its test, followed by the results of the experiments done on the mentioned gold clusters.

II Simulation Foundations

In this section, the foundations of the MD simulation is described and results of tests of their accuracy and/or calibration (e.g., time-steps) are presented. For brevity, some of the implementations are left out entirely. The following components of the MD simulation are dealt with in this section: the Velocity-Verlet Integrator, and the two potential energy models.

II-A Integration Scheme

The MD simulation governs the evolution of the positions and velocities of the atoms in a system with the Velocity-Verlet integration scheme [1]. We present it here for a single atom, but it applies equally to all atoms in a system. Given an atom's mass, m, position, $r(t)$, and velocity, $v(t)$, as well as the length of the time-step, Δt, and a way to compute the forces $f(t)$ and $f(t+\Delta t)$, this method determines the new state of the atom at time $t+\Delta t$. Here the scheme is split into two convenient steps. First, the predictor step:

$$v(t+\Delta t/2) = v(t) + \frac{1}{2m} f(t)\Delta t \tag{1}$$

$$r(t+\Delta t) = r(t) + v(t+\Delta t/2)\Delta t \tag{2}$$

which "predicts" the velocity and updates the position using that prediction. Then the new force is calculated at position $r(t+\Delta t)$, which is used to correct the velocity in the corrector step:

$$v(t+\Delta t) = v(t+\Delta t/2) + \frac{1}{2m} f(t+\Delta t)\Delta t \tag{3}$$

The details of the force calculation rely on the chosen potential energy model. In this project, these energies depend only on the positions of the atoms, so we are guaranteed to be able to calculate the forces for the corrector step using the positions from the predictor step. Note: this means that the predictor step must be computed for all atoms which influence the new force, $f(t+\Delta t)$, *before* the corrector step calculations may begin. In this MD simulation code, this is conveniently accomplished using the vectorized operations of the Eigen library [2].

II-A1 Verlet Test

To test the Verlet Integrator, we compare its results with an analytical solution of the system of differential equations which it is meant to solve:

$$\dot{v}(t) = f(t)/m \tag{4}$$
$$\dot{r}(t) = v(t) \tag{5}$$

It is easily seen that the first equation follows directly from $f(t) = ma(t) = m\dot{v}(t)$, and the second equation is just the definition of velocity as the time-derivative of position.

The general solution of these equations is tricky since we need to know $f(t)$, and that depends on the positions which we are now trying to solve for. However, assuming a constant force, F, on the time interval $[0, T]$, as well as knowledge of the initial position and velocity, $r(0)$ and $v(0)$, we may directly integrate to arrive at:

$$r(T) = \frac{1}{2}FT^2 + v(0)T + r(0) \tag{6}$$
$$v(T) = FT + v(0) \tag{7}$$

C++ functions for the integration of a single and multiple atoms were implemented and tested against the results of the above expressions. Each component of the initial positions, velocities, and forces were set to random values on the interval $[-1, 1]$, and the system was integrated over 10000 time-steps of length $\Delta t = 0.01$. The final position and velocity results for the tests of both functions never differed by more than $1\text{e}{-6}$ of their respective units.

II-B Potential Energy Models

The force, f, on a single atom due to interactions with other atoms is calculated using the potential energy due to the relative positions of other atoms:

$$f = -\frac{\partial E_{\text{pot}}}{\partial r}$$

where E_{pot} is the potential energy model, which depends on the relative positions of the other atoms, and r refers to the position of the atom in question.

The choice of the potential energy model depends on the types of atoms and conditions we wish to simulate. The current MD simulation implements two different models: the Lennard-Jones (LJ) potential, and an Embedded Atom Method (EAM) potential. Here we demonstrate the derivation of the force due to the LJ potential, and discuss the determination of time units for the EAM potential. We also use both potentials to run some simulations to determine the length of quality time-steps, which is judged by how well energy is conserved throughout the simulations.

II-B1 Lennard-Jones Potential

The Lennard-Jones potential describes pairwise interactions between atoms. That is, we will obtain an expression for the force on atom i *due to* atom j. The full force on atom i is then the equal to the sum for all atoms j: $\sum_j f_{ij}$.

a) Force Derivation

The expression we will use for the Lennard-Jones potential is as follows [3]:

$$V(r) = 4\epsilon\left[\left(\frac{\sigma}{r}\right)^{12} - \left(\frac{\sigma}{r}\right)^{6}\right]$$

where σ is a length, ϵ is an energy, and r is the distance between two atoms.

The raw magnitude of the force on atom i due to j is then:

$$\|f_{ij}\| = -\frac{\partial E_{\text{pot}}}{\partial r} \tag{8}$$
$$= -\frac{\partial}{\partial r}4\epsilon\left[\left(\frac{\sigma}{r}\right)^{12} - \left(\frac{\sigma}{r}\right)^{6}\right] \tag{9}$$
$$= -4\epsilon\left[-12\frac{\sigma^{12}}{r^{13}} + 6\frac{\sigma^{6}}{r^{7}}\right] \tag{10}$$
$$= \frac{24\epsilon}{r}\left[2\left(\frac{\sigma}{r}\right)^{12} - \left(\frac{\sigma}{r}\right)^{6}\right] \tag{11}$$

where $r = \|r_{ij}\|$. To give this magnitude the appropriate direction, we simply use it to scale the normalized version of r_{ij}:

$$f_{ij} = \|f_{ij}\|\frac{r_{ij}}{\|r_{ij}\|}$$

Written out in its entirety, the full expression for the force on atom i due to j is then:

$$f_{ij} = \frac{24\epsilon}{\|r_{ij}\|}\left[2\left(\frac{\sigma}{\|r_{ij}\|}\right)^{12} - \left(\frac{\sigma}{\|r_{ij}\|}\right)^{6}\right]\frac{r_{ij}}{\|r_{ij}\|}$$

.

b) Time-Step Determination with LJ

Now we wish to determine an appropriate time-step, which for our purposes means one for which the energy is conserved during a simulation. So, we use the LJ potential and the Velocity-Verlet integrator to simulate a system using different time-steps, and compare the resulting total energies over time to see if there is any noticeable drift.

The system for this demonstration is very small, just 54 atoms. We will refer to it as LJ54 (Fig. 1).

Each simulation uses the following parameters for the LJ potential: $\sigma = 1$ length unit and $\epsilon = 1$ energy unit. The mass of each particle is set to 1 mass unit, and the total time of the simulation, $T = 100\sqrt{m\sigma^2/\epsilon}$. Figure 2 shows the total energy over time for each time-step $\Delta t \in \{0.001, 0.005, 0.01\}$, where these time-steps are of course in units of $\sqrt{m\sigma^2/\epsilon}$.

As can be seen in the plot, even with a time-step of $0.01\sqrt{m\sigma^2/\epsilon}$, there is no noticeable drift in total energy for this system at this temperature. For some systems at higher temperatures, it may be necessary to adjust the time-step to better sample the high-velocity trajectories, so that the relevant forces may act before the particles find themselves in explosive configurations (demonstrated below in Sec. II-B2b).

Even though none of the presented time-steps cause a noticeable drift on this time scale, there is an initial jump in the

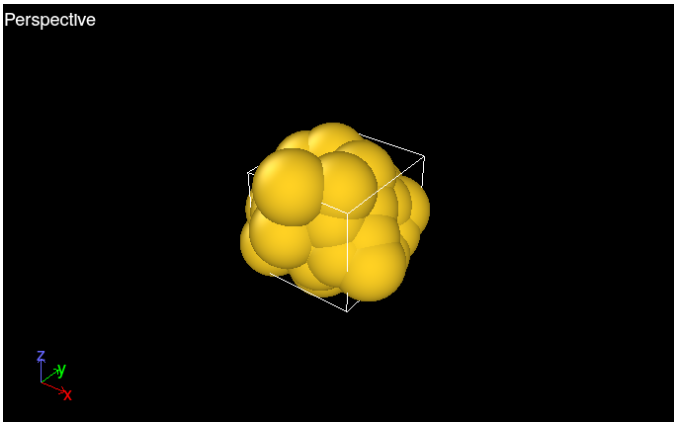

Fig. 1: The initial positions of LJ54, visualized in OVITO [4].

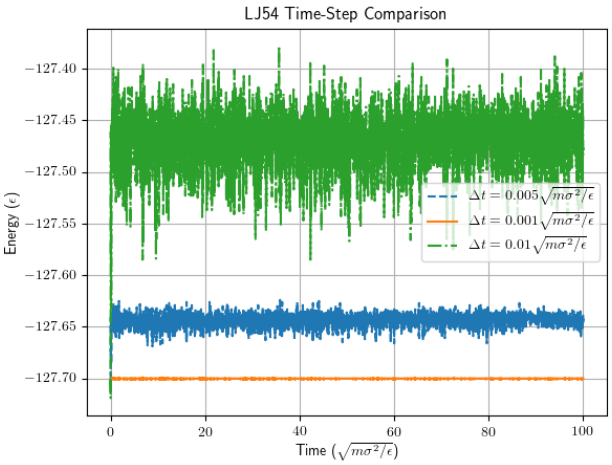

Fig. 2: Plot of total energy vs. time using different time-steps when simulating LJ54. Since the fluctuations make it difficult to distinguish the dash-pattern of each line, the lines represent, in order of lowest line to highest line on the plot: $\Delta t = 0.001$, $\Delta t = 0.005$, and $\Delta t = 0.01$.

energy which seems to grow with increasing time-steps. This may be due to the difference between these time-steps and the time-step with which the system was equilibrated. These time-steps all seem to be safe choices for this system under these conditions, however $\Delta t = 0.001$ is the safest and probably provides a bit more room for exploration of other conditions, e.g., at higher temperatures. Figure 3 shows the final positions of the simulation which used this time-step.

II-B2 Embedded Atom Method Potential

The second inter-atomic potential implemented in this MD simulation is done using an Embedded Atom Method potential. Here we discuss only the units of the simulation when using this potential and determine an appropriate time-step in these units. For more details on the EAM, please see [5].

a) EAM Parameters and Units

The parameters of a model determine its units. In the case of the LJ potential above, the units are fixed by the choice of

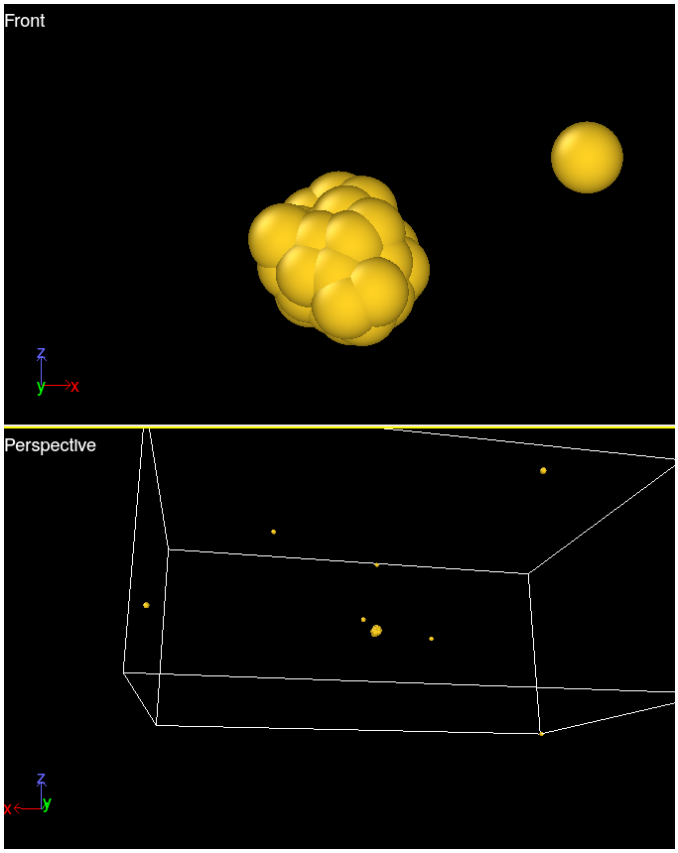

Fig. 3: Visualization of final state of LJ54 ($t = 100\sqrt{m\sigma^2/\epsilon}$) using time-step $\Delta t = 0.001\sqrt{m\sigma^2/\epsilon}$, shown from different angles.

σ, ϵ, and m. In our EAM potential, we take the parameters for the gold atom Au from [6], which fixes our length and energy units as Angstroms (Å) and electron volts (eV), respectively.

In this MD simulation, we choose the units of mass to be g/mol. Therefore, the value of mass for each gold atom when using the EAM potential in this report is 196.96657 g/mol [8]. The choice of mass units in turn fixes the unit of time within the simulation (i.e., the units of time when using the Velocity-Verlet integrator) as 10.18 femtoseconds (fs) [7]. The presentation of the data is adjusted accordingly.

b) Time-Step Determination with EAM

Here we use much the same procedure as in Sec. II-B1b above, however we are now using a Mackay Icosahedron cluster of 923 simulated gold atoms generated with script from [9]). We will refer to this cluster as Cluster923, which was equilibrated to a temperature of 300K before these simulations. Also, to speed computations, a cutoff of 6 Å is imposed on the active length of the potential, beyond which it has no effect. This technique is explained more in Sec. III.

It was mentioned in Sec. II-B1b that a small enough time-step should help ensure that atoms do not find themselves in explosive configurations. Here we demonstrate such a configuration with a simulation using a large time-step of 50 fs. Figure 4 shows the total energy over time. The calculated

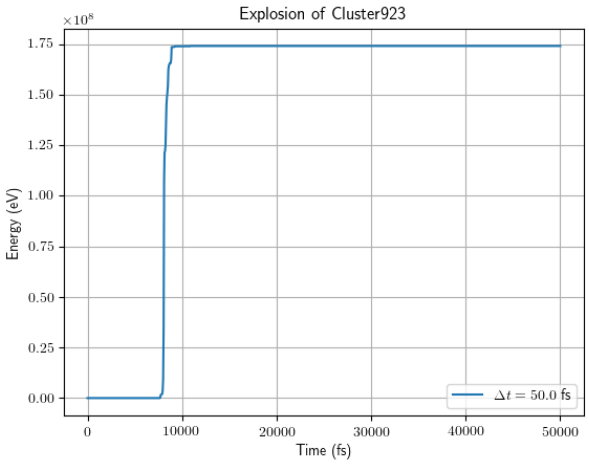

Fig. 4: Plot of total energy during a simulation of Cluster923 using the EAM potential and a time-step of $\Delta t = 50$ fs. Evident is the explosion around time $t = 8000$ fs.

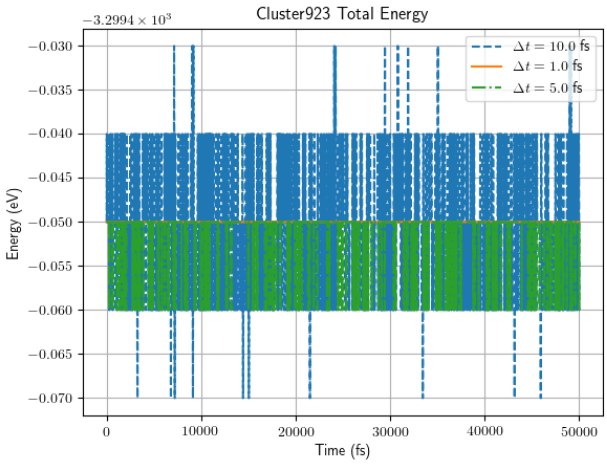

Fig. 5: Total energy plot of Cluster923 with time-steps of 1 fs, 5 fs, and 10 fs, simulated over 50000 fs. The time-step of 1 fs has no visible fluctuations on this plot. It is the horizontal line at -0.05 eV. The other two lines have fluctuations proportional to their time-steps.

initial energy of the system is -3299.45 eV, around which the system stays until about 8000 fs, where the energy and the system explode.

A plausible explanation for this is that the time-step was long enough to allow at least one atom to slip into a region where the repulsive contribution (which grows exponentially with small distances) to the EAM potential exploded, which gave this atom and those it interacted with high enough velocities to increase the chances of this happening again, perhaps with more force, causing a chain reaction.

Now to determine a suitable time-step. Figure 5 shows the comparison of time-steps of 1 fs, 5 fs, and 10 fs. There is no noticeable drift in any of their energies after 50000 fs. The time-step of 5 fs is an acceptable trade-off between computational efficiency and accuracy for the further simulations of this report.

III Computational Techniques

Two techniques are implemented in this MD simulation to significantly speed up the computational process without a significant loss in accuracy. The first is a neighbor list search, which decreases the number of computations performed during a simulation, and the second is that the code is made to run in parallel through a process of domain decomposition.

III-1 Neighbor List Search

The Lennard-Jones interaction is an example of a "short-ranged" interaction, meaning that at a sufficient distance, c, called the cutoff distance, the interaction may be considered negligible. So, for an atom i, we only need to take into account the interactions with atoms j such that $\|r_{ij}\| < c$, where $r_{ij} = r_i - r_j$. For the Lennard-Jones interaction, a reasonable cutoff is $c = 2\sigma$ [3].

To efficiently account for just the atoms within a distance c of an arbitrary atom i (which we call neighbors of atom i) the Neighbor List Search method maintains a neighbor list for each atom throughout the simulation.

To investigate the effect of this method on computational complexity, we use the LJ potential to simulate 10 different lattice clusters, with and without the neighbor list search. We are using the same LJ parameters as before (all are set to 1, including the mass of each particle). The simulations cover a duration of $40\sqrt{m\sigma^2/\epsilon}$ and the time-step used was $0.001\sqrt{m\sigma^2/\epsilon}$. Each lattice was generated using a lattice constant of 1.1σ. The only difference between the lattices in their definition is the number of atoms on one side, s, which takes integer values from 1 to 10. The number of atoms in a lattice then is s^3.

Figure 6 shows the time results (from the "user" output line of the Linux "time" command) vs. the number of atoms for the 10 lattices when simulated without the neighbor list search. These data demonstrate that the complexity of this method is quadratic at best.

Now we repeat the simulations except using the neighbor list method with a cutoff of 2σ. The results are shown in Figure 7. Note that for smaller lattices, the growth appears to be quadratic, but changes to linear for the larger lattices. This is because for smaller lattices, a higher proportion of the atoms find themselves within the average neighbor list, so with small enough lattices with respect to the cutoff, the cutoff has less of an effect on the time complexity.

III-2 Domain Decomposition

The complete exclusion, due to the neighbor list search, of other atoms during a calculation enables us to decompose the system into cells which are only influenced by atoms in neighboring cells. This paves the way for the parallelization of the MD simulation, as each the computation for each cell may be delegated to its own process. Note that since this is

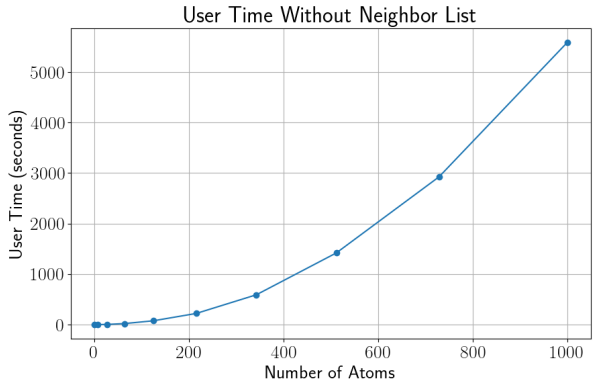

Fig. 6: The user time vs. the number of atoms in a lattice cluster when not using the neighbor list with the LJ potential. Each dot from left to right represents one lattice simulated through $40\sqrt{m\sigma^2/\epsilon}$ using a time-step of $0.001\sqrt{m\sigma^2/\epsilon}$ and the LJ parameters from Sec. II-B1b.

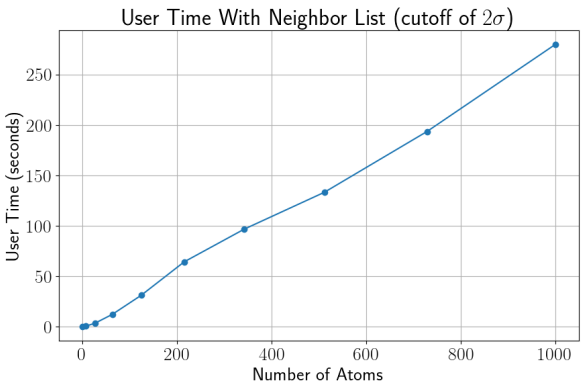

Fig. 7: User time vs. number of atoms for the same lattices from Figure 6, simulated with LJ using the same parameters from Fig. 6, except now with a neighbor list search whose cutoff is 2σ.

only possible with the neighbor list search, it is necessary that the underlying potential is considered short-ranged.

The implementation of this method requires fine attention to detail when it comes to calculating the potential energy, keeping track of the atoms in each cell, and keeping track of an atom's neighbors. To demonstrate that the implementation of this technique is working properly, we ran Cluster923, using the EAM potential, a cutoff of 10 Å , total time of 10000 fs, and a time-step of 1 fs on 1, 2, 4, and 8 MPI processes. Fig. 8 shows the total energy plot of the simulation done on 8 MPI processes. Clearly this simulation is conserving energy, as it did with the other numbers of processes.

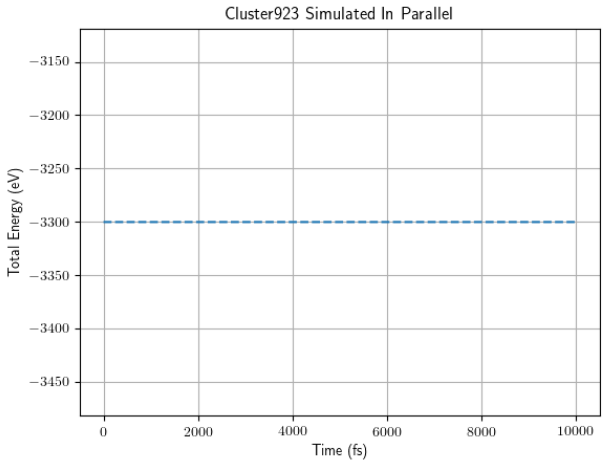

Fig. 8: The total energy plot of Cluster923 simulated for 10000 fs in parallel on 8 MPI processes, with a time-step of 1 fs.

IV Experimental Methods

In this section we present methods used to set up and experiment with the MD simulation. The first sub-section here presents how we may control the temperature of a simulation using the Berendsen thermostat, and the second sub-section expounds an experiment conducted to determine the melting point, heat capacity, and latent heat of gold clusters of various sizes.

IV-1 Berendsen Thermostat

When we introduced Cluster923 in Sec. II-B2b, we mentioned that it had been equilibrated to 300K. This was accomplished using the Berendsen thermostatting scheme [10]. This is a method by which the simulation may add or remove energy to/from the system in order to reach a target temperature. This is accomplished by a gentle rescaling of the velocities which is designed to model a coupling with an external heat bath that is at the target temperature, and a parameter, τ, known as the relaxation constant, may be set which determines the strength of this coupling.

Here we discuss the test strategy of the thermostat. First, a unit test was used to verify that the thermostat was working (at least approximately) by comparing the resulting velocities after one scaling operation with those obtained by using another scaling factor which should be approximately equal to the one used in the Berendsen implementation. The expression for this other scaling factor is the middle expression, left of the approximation symbol in equation 9 of [11].

We believe the above unit test is insufficient for testing the thermostat, since it doesn't even check that the thermostat accomplishes what we intend it to. So, to further test the thermostat we actually equilibrated clusters with it, however this was not done in a unit test.

IV-2 Melting Point of Gold Clusters

In this section we use our MD simulation to investigate the relationship between the sizes of gold clusters and melting

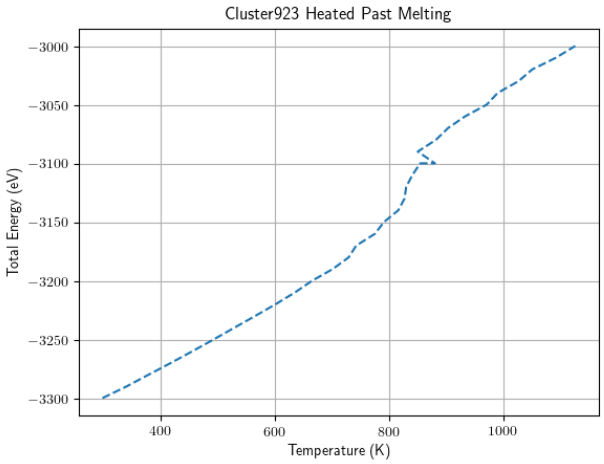

Fig. 9: The averaged total energies and temperatures of Cluster923 as it was gradually heated past its melting point by the process described in IV-2, where the simulation parameters are also given.

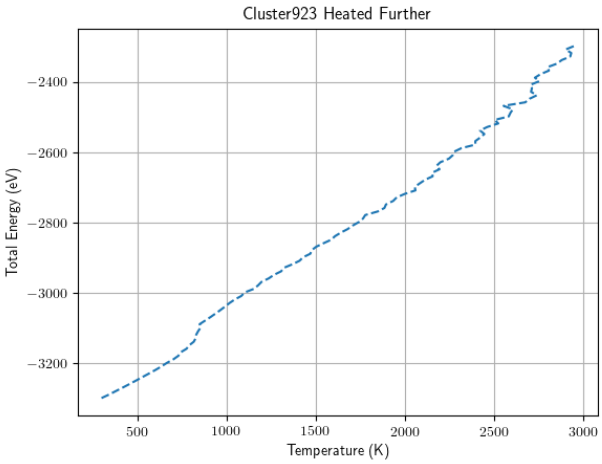

Fig. 10: Repeated experiment from Fig. 9, but for 100 iterations of heating process to ensure that the phase transition had completed.

point, latent heat, and heat capacity. The process for each cluster is as follows:

1) The cluster is first equilibrated to 300 K.
2) The total energy and temperature is recorded.
3) The cluster's energy is incremented by ΔQ eV.[1]
4) The cluster is left to relax for 5000 fs. Over the final 2500 fs of this, the average temperature and average total energy of the cluster is taken.
5) The process is repeated from Step 2 as necessary.

We first present a plot of the mentioned averages of total energy average vs temperature for Cluster923, heated past melting point. These simulations used a time-step of 5 fs and the EAM potential with a neighbor list cutoff of 6 Å. Fig. 9 plots the resulting averages when the process is repeated 30 times, using $\Delta Q = 10$ eV.

Immediately evident is the sudden behavioral change from a nice linear relationship (during which the slope was calculated from the data to be 0.2672 eV/K) to even violating the mathematical definition of function. This is due to a change in phase of the cluster (and noise due to fluctuations of the total energy/temperature which may have not been sufficiently removed by the averaging process). During the linear portion, the slope was calculated from the data to be 0.2672 eV/K, which represents the heat capacity of this cluster.

To be sure that this cluster was melted, the experiment was repeated, this time for 100 iterations of the heating process. The result is shown in Fig. 10. One can see again the linear initial portion, followed by the first phase transition, after which the overall slope of the curve is similar to that of the linear portion. The cluster began to vaporize around iteration 66 of the heating process, which corresponds to temperatures around 2153.5 K, and coincides with the increase in fluctuations on the plot, another phase transition.

Now we present the calculation of latent heat from the data of the 2nd experiment (shown in Fig. 10). We judged when the transition began by looking at the visualizations in OVITO at temperatures around the break in linearity in the plot (the beginning of an almost temperature plateau), and placed the beginning of the phase transition where the temperature was 827.073 K and the total energy was -3129.29 eV. The end of the temperature plateau is where the temperature is 849.387 K and the energy is -3089.18 eV. Therefore the calculated latent heat for this cluster is 40.1 eV. The melting point is determined as the middle of this temperature interval: 838.23 K.

The same procedure was followed to determine the same quantities for different cluster sizes. A plot of the melting point vs. cluster size is given in Fig. 11. A similar plot for heat capacity is Fig. 12, and for latent heat in Fig. 13.

One would expect that the melting points should not change, as the melting point of gold is irrespective of the size. However, this typically refers to clusters of gold orders of magnitude larger than the ones presented here. This project illuminates how melting point and other thermodynamic properties are statistical in nature.

V Conclusion

In this report, we have presented a comprehensive overview of a Molecular Dynamics (MD) simulation. We discussed the foundational aspects of the simulation, including the Velocity-Verlet integration scheme and the implementation of the Lennard-Jones and Embedded Atom Method potentials. We also addressed the crucial issue of time-step determination for each potential and the choice of units.

[1]This is done by scaling the velocities by a factor of $\lambda = \sqrt{\frac{K+\Delta Q}{K}}$, where K is the kinetic energy before the scaling. This achieves the desired result, since the new velocity of atom i is λv_i, the kinetic energy of the system after scaling is $\frac{1}{2}m\sum_i(\lambda v_i)^2 = K + \Delta Q$, where v_i is the velocity of atom i before scaling.

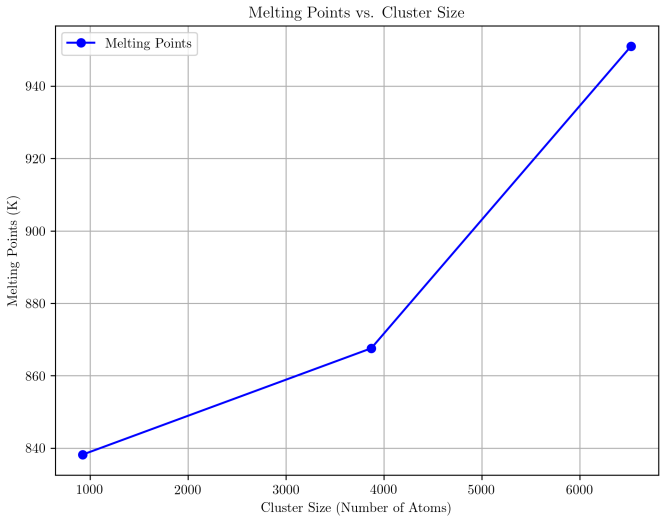

Fig. 11: Plot of melting points vs. cluster size for clusters of sizes 923, 3871, and 6525 atoms.

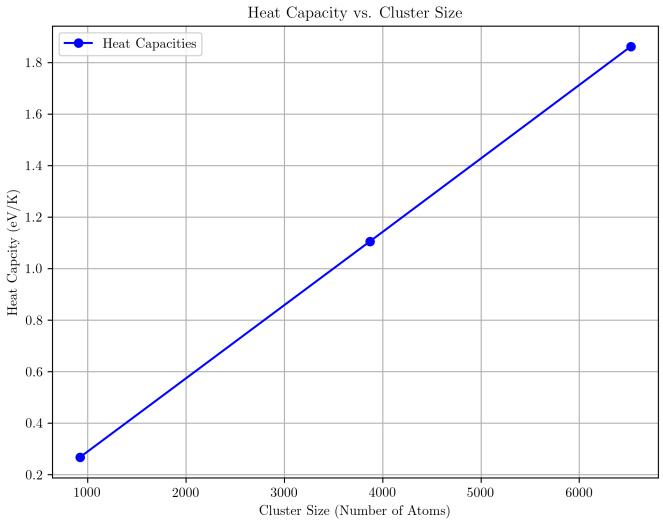

Fig. 12: Heat capacity vs. cluster size for clusters of sizes 923, 3871, and 6525 atoms.

Furthermore, we highlighted two essential computational techniques: the neighbor list search and domain decomposition, which significantly improved the efficiency of the MD simulation. These techniques were demonstrated to be effective in improving computational complexity and enabling parallelization.

In the experimental section, we discussed the Berendsen thermostat for temperature control and conducted experiments to determine the melting point, heat capacity, and latent heat of gold clusters of varying sizes.

Overall, the MD simulation and experimental investigations have contributed to a better understanding of the thermodynamic properties of gold clusters.

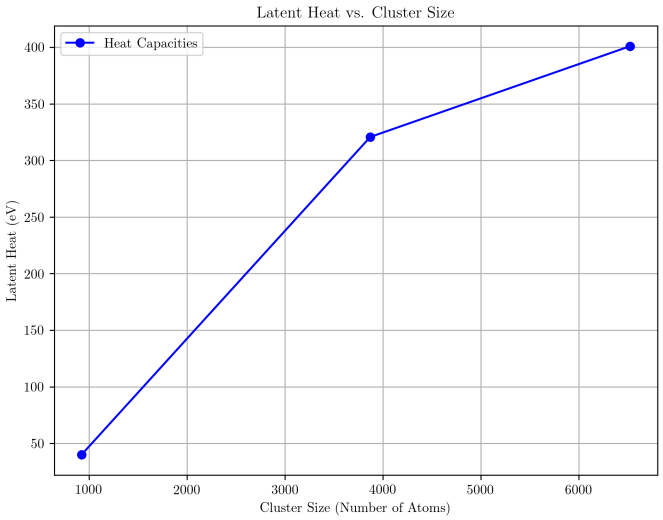

Fig. 13: Latent Heat vs. cluster size for clusters of sizes 923, 3871, and 6525 atoms.

Acknowledgments

I would like to express my sincere gratitude to the following individuals for their invaluable help and support during the completion of this project:

- Lars Pastewka
- Ibrahim Ghanem
- Lucas Frèrot

I really enjoyed overcoming the challenges of the engaging class you all have provided, and I am looking forward to honing my new skills to apply them to the challenges of the future. Thank you.

References

[1] Pastewka, L. Chapter 02. Molecular Dynamics. https://pastewka.github.io/MolecularDynamics/_lecture/chapter02.html (accessed 2023-08-30).

[2] Eigen. eigen.tuxfamily.org. https://eigen.tuxfamily.org/index.php?title=Main_Page#Credits.

[3] Pastewka, L. Chapter 03. Molecular Dynamics. https://pastewka.github.io/MolecularDynamics/_lecture/chapter03.html (accessed 2023-08-31).

[4] OVITO – Open Visualization Tool – Scientific visualization and analysis software for atomistic simulation data. https://www.ovito.org/.

[5] Pastewka, L. Chapter 05. Molecular Dynamics. https://pastewka.github.io/MolecularDynamics/_lecture/chapter05.html (accessed 2023-08-31).

[6] Cleri, F.; Rosato, V. Tight-Binding Potentials for Transition Metals and Alloys. Physical Review B 1993, 48 (1), 22–33. https://doi.org/10.1103/physrevb.48.22.

[7] Pastewka, L. eV/Å units. Molecular Dynamics. https://pastewka.github.io/MolecularDynamics/_notes/eV_A_units (accessed 2023-08-31).

[8] Standard Atomic Weights — Commission on Isotopic Abundances and Atomic Weights. www.ciaaw.org. https://www.ciaaw.org/atomic-weights.htm.

[9] Wang, Y. Mackay Icosahedron Structure Generator. www.pas.rochester.edu. https://www.pas.rochester.edu/~wangyt/algorithms/ih/ (accessed 2023-08-31).

[10] Berendsen, H. J. C.; Postma, J. P. M.; van Gunsteren, W. F.; DiNola, A.; Haak, J. R. Molecular Dynamics with Coupling to an External Bath. The Journal of Chemical Physics 1984, 81 (8), 3684–3690. https://doi.org/10.1063/1.448118.

[11] Pastewka, L. Chapter 04. Molecular Dynamics. https://pastewka.github.io/MolecularDynamics/_lecture/chapter04.html (accessed 2023-09-01).